Laser Physics

PAPER

Supercontinuum generation in photonic crystal fibers infiltrated with nitrobenzene

IOP Publishing | Astro Ltd Laser Physics

Laser Phys. **30** (2020) 035105 (9pp) https://doi.org/10.1088/1555-6611/ab6f09

Supercontinuum generation in photonic crystal fibers infiltrated with nitrobenzene

Lanh Chu Van[1], Van Thuy Hoang[2,3], Van Cao Long[4], Krzysztof Borzycki[5], Khoa Dinh Xuan[1], Vu Tran Quoc[1], Marek Trippenbach[2], Ryszard Buczyński[2,3] and Jacek Pniewski[2]

[1] Department of Physics, Vinh University, 182 Le Duan, Nghe An Province, Vinh City, Vietnam
[2] Faculty of Physics, University of Warsaw, Pasteura 5, 02-093 Warsaw, Poland
[3] Department of Glass, Institute of Electronic Materials Technology, Wólczyńska 133, 01-919, Warsaw, Poland
[4] Institute of Physics, University of Zielona Góra, Prof. Szafrana 4a, 65-516 Zielona Góra, Poland
[5] National Institute of Telecommunications, Szachowa 1, 04-894 Warsaw, Poland

E-mail: j.pniewski@uw.edu.pl

Received 16 August 2019
Accepted for publication 20 January 2020
Published 14 February 2020

Abstract

A photonic crystal fiber made of fused silica glass and infiltrated with nitrobenzene ($C_6H_5NO_2$) was proposed as a new nonlinear medium for supercontinuum generation (SG). The guiding properties of the fiber structure were studied numerically, including estimation of the effective refractive index, attenuation, and dispersion of the fundamental mode. Based on the obtained results, three optimized structures were selected and tested numerically for SG. With numerical simulations of nonlinear propagation, we demonstrated the feasibility of spectrally broad and coherent SG in the proposed structures. For the first we obtained a supercontinuum (SC) in the range of 0.8–1.8 μm, for the second in the range of 0.8–2.1 μm, and for the third 1.3–2.3 μm. The pulse energy was in the range of 0.06–0.5 nJ while the pulse duration was 90 fs or 120 fs. For all structures an SC was formed in the first centimeter of the light propagation and conveniently allowed to assume short segments of the fibers. The proposed fibers are good candidates for all-fiber SC sources constituting an attractive alternative to glass-core fibers, since the nonlinearity of nitrobenzene is significantly higher than that of silica. The proposed solution may lead to new low-cost all-fiber optical systems for SG.

Keywords: photonic crystal fibers, nitrobenzene, supercontinuum generation, dispersion, nonlinear optics

(Some figures may appear in colour only in the online journal)

1. Introduction

The invention of photonic crystal fibers (PCFs) by Knight *et al* [1] gave rise to a new class of fibers with unique optical properties, such as single-mode guidance [2, 3], birefringence [4], and the possibility to tailor dispersion characteristics [5, 6], which are crucial for efficient supercontinuum generation (SG). New types of PCFs have been presented, such as large-mode area fibers [7] and all-solid fibers [8], and have all led directly to practical applications, e.g. sensors [9], lasers [10], and supercontinuum (SC)-based light sources [11].

PCFs can have air holes in the cladding and/or in the core that provide different light-guiding regimes. The infiltration of PCFs with specific liquids or gases allows for tuning the linear and nonlinear optical properties of PCFs, thus enhancing the range of applications [12, 13]. Further modifications of guiding properties of the fibers on the fly are possible with the application of an external electric field [14] or temperature tuning [15].

For efficient SG flat dispersion characteristics in both the normal and anomalous dispersion regime are required. These can be obtained by the proper structure of PCF and type of

Table 1. Pulse parameters and SC range obtained in selected PCFs from our previous works.

Liquid	Pulse length (fs)	Pulse wavelength (μm)	Pulse energy (nJ)	Fiber length (cm)	SC range (μm)	Regime	Reference
C_7H_8	350	1.55	2.5	4–5	1.1–1.75	Normal	[20]
C_7H_8	450	1.55	3	4–5	1.0–1.75	Anomalous	[20]
C_7H_8	400	1.03	10	10	0.95–1.1	Normal	[30]
CCl_4	300	1.35	0.8	30	0.8–1.9	Anomalous	[22]
CCl_4	300	1.064	0.8	30	0.95–1.15	Normal	[22]
CCl_4	300	1.55	0.8	30	1.05–1.75	Anomalous	[22]
CCl_4	400	1.03	25	20	0.85–1.25	Normal	[31]
$CHCl_3$	400	1.03	1	10	0.6–1.26	Normal	[26]
$CHCl_3$	400	1.03	1	10	0.6–1.4	Anomalous	[26]

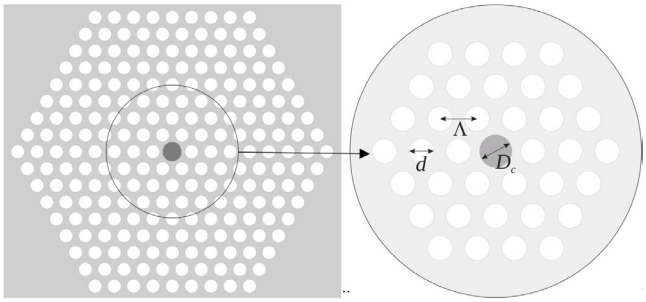

Figure 1. Schematic picture of the modeled PCF structure. Coefficient D_c is the diameter of the liquid-filled core and d represents the diameter of the air-filled core.

infiltrating liquid. SG in liquid-filled PCFs has been presented by several groups, and carbon disulfide (CS_2), toluene (C_7H_8), carbon tetrachloride (CCl_4), ethanol (C_2H_5OH), and chloroform ($CHCl_3$) have been shown to be suitable nonlinear liquids for efficient spectral broadening [16–28]. These liquids have a nonlinear refractive index n_2 higher than that of fused silica (even up to 200 times for CS_2) and are transparent in the visible and near-infrared (NIR) range, although some of them are highly toxic and hence have limited applicability. It is worth stressing that n_2 depends on the pumping pulse width. For very short pulses shorter than 50 fs, only the bound electronic nonlinearity contributes significantly to n_2, while for long pulses, at the level of tens of ps, the vibrational and reorientational responses also contribute and may even become dominant, thus increasing the effective n_2. For instance, for CS_2, n_2 in the range of $1–20 \cdot 10^{-19}$ m^2 W^{-1} was already reported [29].

Many different PCF structures and filling strategies have already been studied. For example, Vieweg *et al* demonstrated a two-photon direct-laser writing technique that allows for the closing of individual air holes in a PCF. It allows for SG when infiltrated with CCl_4 and a femtosecond pump is used (210 fs long pulses with a center wavelength of 1.03 μm). They achieved a 600 nm wide SC spectrum when a beam power of 100 mW was used [16]. Later, a theoretical design of a liquid-filled PCF was presented, where only one ring of holes surrounding the core was filled with a hypothetical liquid. As a result, near-zero ultra-flat dispersion as small as 0 ± 0.41 ps $\cdot$ nm$^{-1} \cdot$ km^{-1} for a broad wavelength range and SC in the 400 nm wide range was shown, although given within relatively large dynamics of 100 dB [17].

It has already been demonstrated that a spectrally broad SG is possible using liquids such as CS_2 [18, 19, 24], toluene [20], ethanol [21], carbon tetrachloride [22, 25], and chloroform [26–28]. More complicated theoretical PCFs were also proposed, e.g. those using a mixture of two different liquids [23].

Table 2. Sellmeier's coefficients for the materials used.

Coefficient	Value
Fused silica	
B_1	0.6694226
B_2	0.4345839
B_3	0.8716947
C_1	4.4801×10^{-3} μm^2
C_2	1.3285×10^{-2} μm^2
C_3	95.341482 μm^2
Nitrobenzene	
B_1	1.30628
B_2	0.00502
C_1	0.02268 μm^2
C_2	0.18487 μm^2

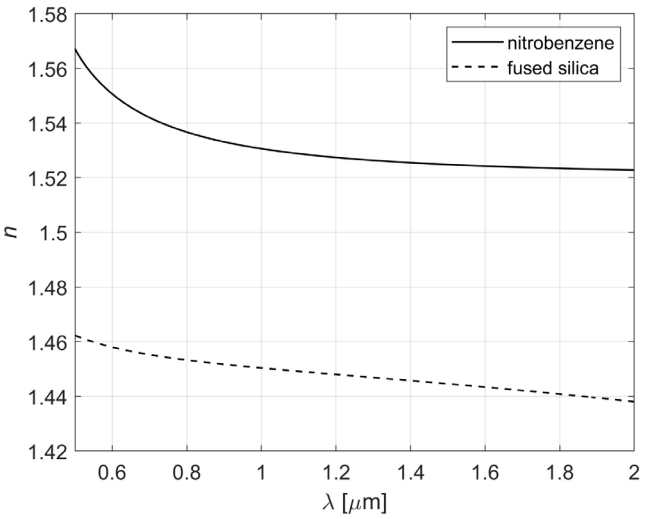

Figure 2. Characteristics of the real part of the refraction index of nitrobenzene and fused silica [32].

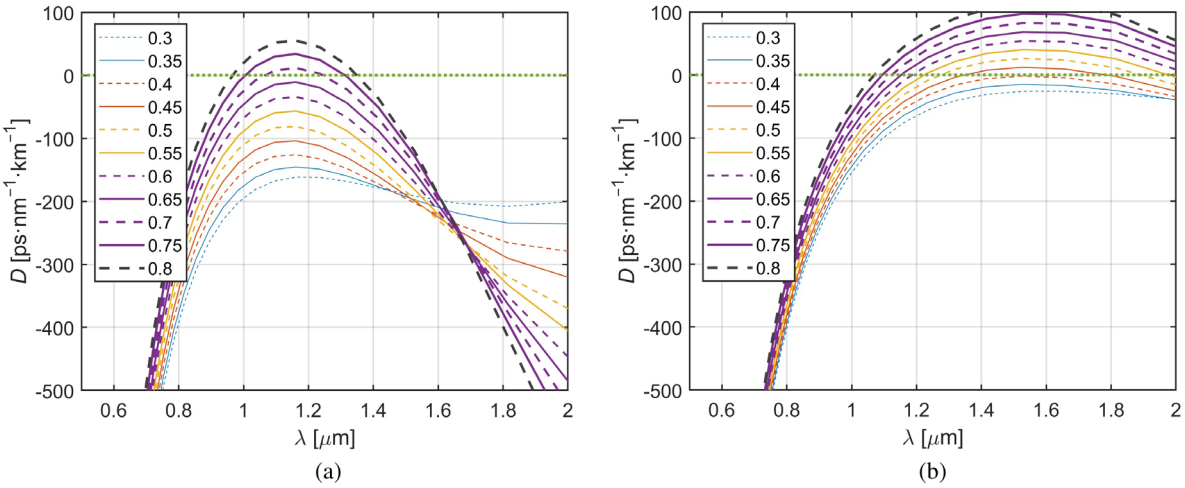

Figure 3. Characteristics of the PCF mode dispersion for f values in the range from 0.3 to 0.8 and (a) $\Lambda = 1.0$ μm, (b) $\Lambda = 1.5$ μm.

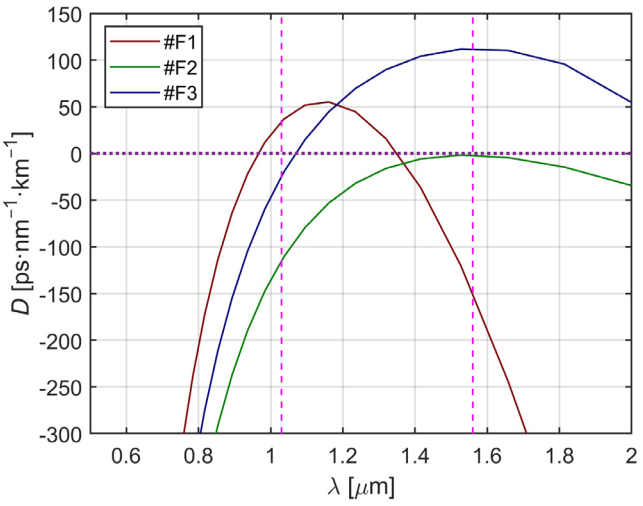

Figure 4. Characteristics of PCF mode dispersion for the fibers $\#F_1$, $\#F_2$, and $\#F_3$. The dashed vertical lines indicate the pump wavelengths 1030 nm and 1560 nm, respectively.

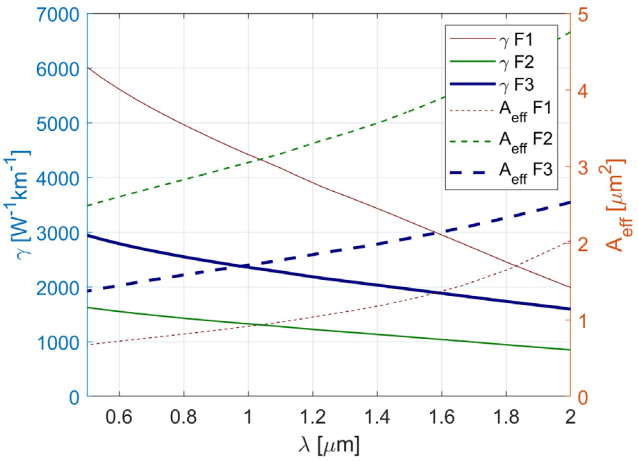

Figure 5. The effective nonlinear coefficient γ and the mode area A_{eff} of the fibers $\#F_1$, $\#F_2$, and $\#F_3$.

Table 3. Nonlinear parameters used in simulations [29]. The subscripts *el*, *d*, *l*, *c* indicate the bound-electronic, molecular reorientation, molecular interaction and collision-induced mechanisms, respectively.

Parameter	Value
$n_{2,el}$	$0.60 \cdot 10^{-19}$ m^2 W^{-1}
$n_{2,d}$	$5.00 \cdot 10^{-19}$ m^2 W^{-1}
$\tau_{r,d}$	0.1 ps
$\tau_{f,d}$	3.5 ps
$n_{2,l}$	$1.7 \cdot 10^{-19}$ m^2 W^{-1}
$n_{2,c}$	$0.35 \cdot 10^{-19}$ m^2 W^{-1}
$\tau_{r,c}$	0.2 ps
$\tau_{f,c}$	0.1 ps

In this paper we analyze a PCF made of fused silica glass, with a nitrobenzene-filled core in the context of the centimeter-long NIR SC source pumped with low-energy femtosecond laser pulses. The guiding properties of the proposed fibers in terms of the effective refractive index, attenuation, and dispersion of the fundamental mode were studied and optimized setups were selected and analyzed in detail. Coherent and non-coherent SG has been numerically obtained, depending on the pump and fiber structure parameters.

In our study we were solving the generalized nonlinear Schrödinger equation (GNLSE) searching for the SG. Our results will be summarized below, but first, to get the proper framework we present the results of our previous studies. In table 1, we display the characteristics of the optimized PCFs with the cores infiltrated with different liquids with the view of application in all-fiber low-pulse energy systems.

2. Numerical modeling of the PCF

The schematic view of the geometrical structure of the modeled PCF is shown in figure 1. We assume that the PCF is made of fused silica glass (SCHOTT Lithosil®). It consists of eight

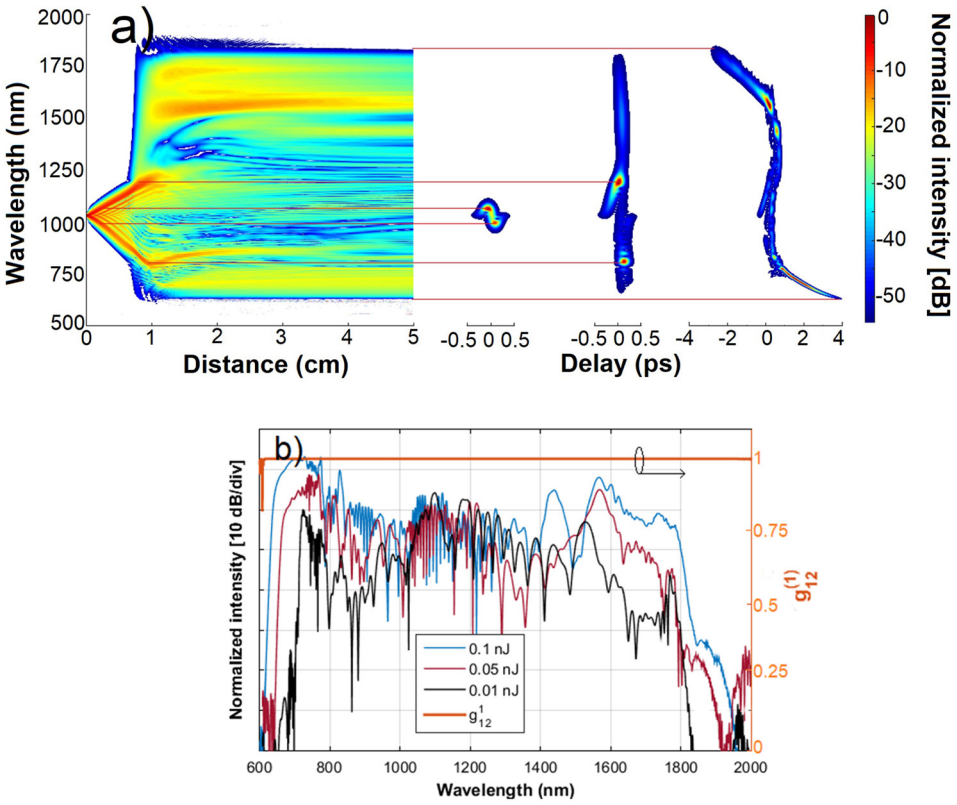

Figure 6. (a) Evolution of the SC along the fiber; (b) SC spectrum for different pulse energies in the range of 0.01–0.1 nJ and degree of coherence calculated from 20 individual pairs with random noise for the pulse energy 0.1 nJ, for $\#F_1$.

rings of air holes ordered in a hexagonal lattice, surrounding the central nitrobenzene-filled hole. Nitrobenzene is a water-insoluble pale yellow oil with a specific odor of almonds. The linear filling factor of the cladding is defined as $f = d/\Lambda$, where d is the diameter of a single air hole, and Λ is the lattice constant. Figure 2 depicts the characteristics of the real part of the refractive index of nitrobenzene compared to fused silica glass. According to the measurements in [32] nitrobenzene is transparent in the visible and NIR range with an absorption maximum at 1.67 μm. The refractive index characteristics are modeled using Sellmeier's equation as given below, where the C_i coefficients have dimensions of micrometers squared (μm^2)

$$n^2(\lambda) = A_1 + \frac{B_1\lambda^2}{\lambda^2 - C_1} + \frac{B_2\lambda^2}{\lambda^2 - C_2} + \frac{B_3\lambda^2}{\lambda^2 - C_3}. \quad (1)$$

Sellmeier's coefficients for fused silica and nitrobenzene are presented in table 2.

3. Modeling modal and dispersion properties of the PCF

First, preliminary numerical simulations were conducted for $\Lambda = 1.0$ μm and $\Lambda = 1.5$ μm and for filling factors in the range of 0.3–0.8. For each simulation run the diameter of the core was calculated from the equation $D_c = 2\Lambda - 1.1d$. The smallest core diameter was 1.12 μm for $\Lambda = 1.0$ μm and $f = 0.8$. The biggest core diameter was 2.67 μm for $\Lambda = 1.5$ μm and $f = 0.3$. A commercial-grade eigenmode solver was used to perform the calculations in case of modal and dispersion properties of the PCF [33], with the assumption that nitrobenzene exhibits negligible losses. This assumption does not influence dispersion characteristics, which are taken into account in all simulations.

The holes in the first ring surrounding the core have the leading influence on the dispersion properties of the fiber, including zero dispersion wavelength (ZDW). The other rings are mainly responsible for mode attenuation, especially for higher modes [34]. In the modeling, a constant filling factor for all rings was assumed, in order to simplify future fiber development. We did not verify whether the selected fiber was single-mode or multi-mode. This analysis was only performed for optimized fibers. In figures 3(a) and (b) characteristics of dispersion for the fundamental mode are shown for the wavelength range 0.5–2 μm.

On the basis of numerous numerical simulations three fibers were selected; we call them $\#F_1$, $\#F_2$, and $\#F_3$. For the fiber $\#F_1$ $\Lambda = 1.0$ μm and $f = 0.8$. This fiber is intended for SG in the anomalous regime of dispersion while pumped at 1030 nm. The dispersion is equal to 33.7 ps $\cdot$ nm^{-1} $\cdot$ km^{-1} at the pump wavelength. The fiber has two ZDWs around 960 nm and 1345 nm. For the fiber $\#F_2$ $\Lambda = 1.5$ μm and $f = 0.4$. This fiber is expected to generate an SC in an all-normal range of dispersion. At the planned pump wavelength 1.56 μm the dispersion is equal -2.2 ps $\cdot$ nm^{-1} $\cdot$ km^{-1}. For the fiber $\#F_3$ $\Lambda = 1.5$ μm and $f = 0.8$. In this case, the pump wavelength 1.56 μm is located in the anomalous regime of dispersion.

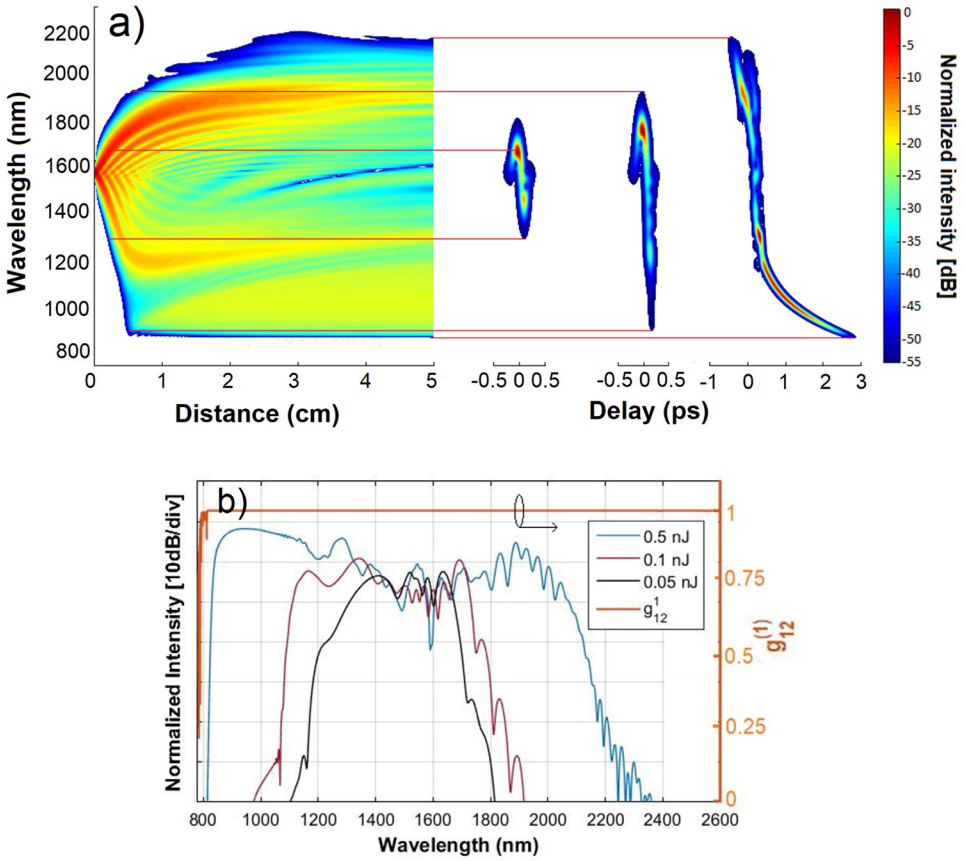

Figure 7. (a) Evolution of the SC along the fiber; (b) SC spectrum for different pulse energies in the range of 0.05–0.5 nJ and degree of coherence calculated from 20 individual pairs with random noise for the pulse energy 0.5 nJ, for $\#F_2$.

Figure 4 depicts the dispersion characteristics for these three fibers.

The effective nonlinear coefficients γ for the fibers $\#F_1$ and $\#F_2$ and their effective mode areas are shown in figure 5. The coefficient γ is calculated from the equation $\gamma = n_2\omega_0/cA_{eff}$, where ω_0 is the central frequency of the pulse, c is the speed of light in the vacuum, and A_{eff} is the effective mode area of the fiber for the fundamental mode. All three structures are effectively single-mode since other modes have attenuation at least two orders of magnitude higher than the fundamental or are located in the cladding.

4. SG in selected fibers

The nonlinear properties of the investigated fibers are calculated numerically solving the GNLSE, using the split-step Fourier method [35]

$$\partial_z\tilde{A} = i\tilde{\beta}(\omega)\tilde{A} - \frac{\tilde{\alpha}(\omega)}{2}\tilde{A} + i\frac{n_2(\omega_0)\,\omega}{cA_{eff}(\omega)}\tilde{A}\mathcal{F}\left[\int_{-\infty}^{\infty} R(t')\,|A|^2(t-t')\,dt'\right], \quad (2)$$

where $\tilde{A}(\omega)$ is the Fourier transform (FT) of an envelope pulse $A(t)$. The influence of the dispersion characteristic $\beta(\omega)$ on the nonlinear properties of the fiber is described by the first term on the right-hand side of equation (2), and $\tilde{\beta}(\omega) = \beta(\omega) - (\omega-\omega_0)\beta_1 - \beta_0$. The term $\tilde{\alpha}(\omega)$ is the FT of the attenuation coefficient $\alpha(t)$. In the simulations, the attenuation term is approximated by the sum of confinement and material loss. The nonlinear response function $R(t')$ is a sum of electronic-bound and molecular contributing mechanisms and can be defined as in the equation below, where $N = n_{2el} + n_{2c} + n_{2d} + n_{2l}$ [36]

$$R(t') = \frac{1}{N}\left[2n_{el} + \left(n_{2l}C_{2l}e^{-t'/t_{fl}}\int_0^{\infty}\frac{\sin(\omega t')}{\omega}g(\omega)\,d\omega + \sum_{k=c,d} n_{2k}C_{2k}\left(1-e^{-t'/t_{rk}}\right)e^{-t'/t_{fk}}\right)\Theta(t')\right]. \quad (3)$$

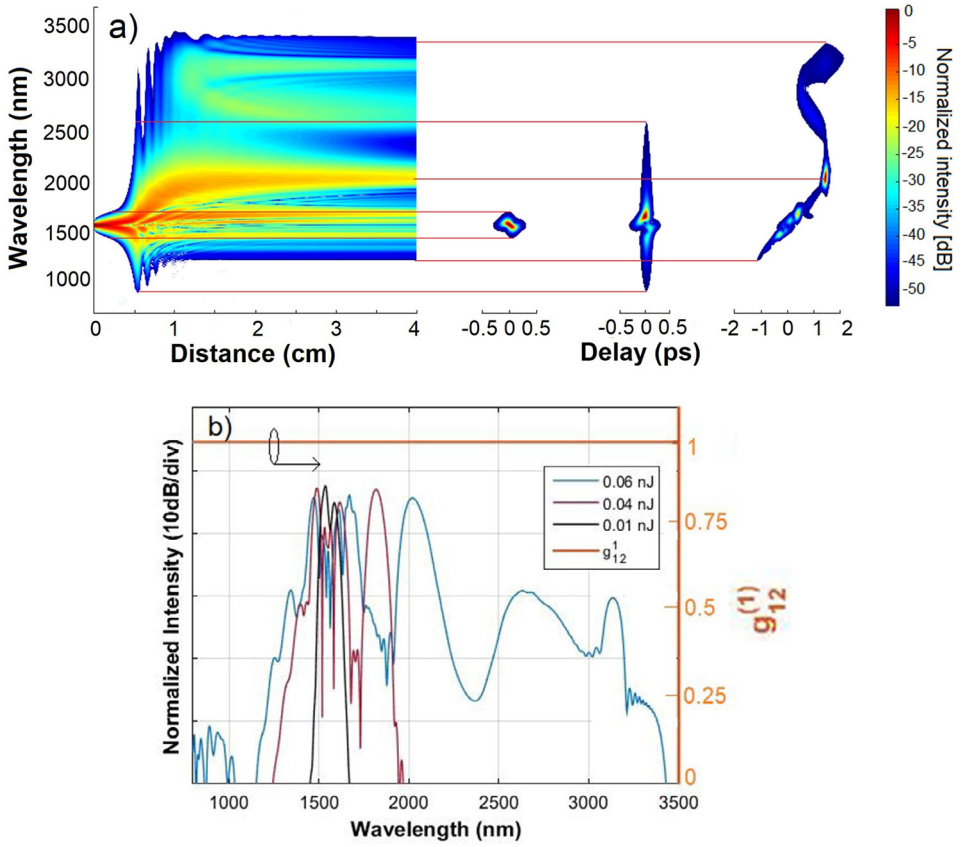

Figure 8. (a) Evolution of the SC along the fiber; (b) SC spectrum for different pulse energies in the range of 0.01–0.06 nJ and degree of coherence calculated from 20 individual pairs with random noise for the pulse energy 0.06 nJ, for $\#F_3$.

Table 3 presents the values of all respective parameters.

The coherence characteristics of the fibers investigated in our model take into account shot noise and spontaneous Raman scattering. Because the first-order coherence has a more straightforward interpretation in terms of classical optics, it will be used to discuss noise-related issues. The coherence characteristics are calculated numerically using equation (4) [37] for ensembles of the corresponding SC spectra

$$\left|g_{12}^{(1)}\left(\lambda, t_1 - t_2 = 0\right)\right| = \left|\frac{E_1^*\left(\lambda, t\right) E_2\left(\lambda, t\right)}{\left[\left|E_1\left(\lambda, t\right)\right|^2 \left|E_2\left(\lambda, t\right)\right|^2\right]^{1/2}}\right|. \quad (4)$$

For $\#F_1$ the pulses have central wavelength 1030 nm and duration 120 fs, which is available upon using the Menlo Systems femtosecond ytterbium fiber laser. The evolution of the SC is simulated over a propagation distance of 5 cm with input pulse energy 0.1 nJ, which corresponds to the peak power 0.83 kW. SG is demonstrated in figure 6. At the beginning of propagation, self-phase modulation (SPM) has a dominant contribution to spectral broadening. The new wavelengths, generated by SPM, act as a seed source for four-wave mixing (FWM). We notice that, similarly to a fiber with single ZDW, the dispersive wave plays the key role in the generation of new wavelengths at the blue side of the spectrum around 700 nm (close to the short-wavelength ZDW). Also, the combination of the negative value of the dispersion slope and anomalous dispersion regime lead to the red-shifted dispersive wave, resulting in the new long wavelengths generated at the leading edge of the spectrum, around 1700 nm (figure 6(a)) [35, 38]. The dispersive waves play significant roles in spectral broadening at the edges of the spectrum, while the soliton fission (SF) is suppressed and occurs only at the central area of the SC spectrum. The cut-down of the contribution of SF to spectral broadening should decrease the noise of the SG and improve the coherence. The slope of the dispersion also restricts the spectral broadening, and increasing the input pulse energy does not provide significant further spectral bandwidth broadening. Figure 6(b) shows the SC spectrum for different pulse energies and the numerical calculation of first-order coherence of SG.

For $\#F_2$ the pulses have central wavelength 1560 nm and duration 90 fs, which is available in, e.g. Menlo Systems C-fiber femtosecond erbium laser. The evolution of the SC is simulated over a propagation distance of 5 cm with input pulse energy 0.5 nJ, which corresponds to the peak power 5.55 kW. The SG is shown in figure 7. Due to the high nonlinear coefficient γ, in the case $\#F_2$, the spectral broadening occurs rapidly in the first centimeter of the propagation length, and the expected spectral bandwidth can be obtained at a short length of the fiber. As shown in figure 7(a), at the beginning SPM is the dominant contribution to the spectral broadening. Due to the self-steepening, the SC spectrum is asymmetric with respect to the pump wavelength and there is the tendency of spectral broadening towards the blue side of the spectrum. In the normal dispersion regime, the newly created wavelength

components by SPM at the trailing edge with a high amount of dispersion move slower than the pulse tail at the center of the pulse. This leads to the mixing of the new components with the pulse tail, resulting in the onset of optical wave breaking. The overlap of the temporal component of these tails leads to the generation of new wavelengths by FWM. The components at 1200 nm act as a pump and the tail of the pulse at 1560 nm as the seed. As a result, the wavelength induced by FWM is around 975 nm. The relation between these components follows [39]

$$\omega_{FWM} = 2\omega_{pump} - \omega_{seed} \Leftrightarrow \frac{1}{\lambda_{FWM}} = \frac{2}{\lambda_{pump}} - \frac{1}{\lambda_{seed}}. \quad (5)$$

The component with new wavelengths from FWM results in optical wave-breaking (OWB), and thus, OWB occurs in the trailing edge and generates new wavelengths around 800 nm. During further propagation, the slope of dispersion at the blue side of the spectrum restricts the spectral broadening. The fiber has a low amount of normal dispersion at the leading edge and high attenuation, thus OWB does not occur at the leading edge of the pulse. The temporal profile remains flat at the trailing edge even at longer propagation distance. Finally, the all-normal dispersion SC spectrum extends from 800 to 2100 nm within a 20 dB dynamic range. According to [40], SG in the all-normal dispersion regime has a potential for high coherence (figure 7(b)).

For $\#F_3$ the pulses have central wavelength 1560 nm and duration 90 fs. The pulse evolution is simulated over a propagation distance of 5 cm with input pulse energy 0.06 nJ, which corresponds to the peak power 0.66 kW. The SG is shown in figure 8. The spectral broadening is induced by SPM at the beginning of the propagation in the fiber. SF occurs at around 0.5 cm and is accompanied by the creation of Raman solitons. At the same time, soliton breathing [41, 42] leads to sudden spectral broadening and generates new wavelength components up to 3500 nm (across the ZWD) at the leading edge and around 1000 nm at the trailing edge. If the pulses have sufficient peak power the new wavelengths generated by soliton breathing create a dispersive wave. As shown in figure 8(a), the dispersive wave is generated at around 1 cm of propagation distance at the leading edge (around 3500 nm). The dispersive wave also appears and generates short wavelength components (around 1000 nm) with bigger input pulse energy. The expected spectral bandwidth is achieved after the propagation of 1 cm. During further propagation in the fiber, the generated spectrum remains constant.

The numerical analysis in this work pointed out that the investigated SC pulses have the potential for high coherence with first-order coherence equal to 1 over the entire width of their spectral characteristics. The coherence of SG in optical fibers depends on a lineup of factors, i.e. contribution of Raman scattering, polarization noise, laser shot noise, but also fiber length and input (pump) soliton order [43–45]. In particular, it has been shown that lowering the dispersion and peak power of the input pulse would contribute to limiting the Raman noise [43]. Polarization noise can be suppressed by the use of a birefringent fiber [44]. Laser shot noise related to amplitude fluctuation of individual laser pulses compared to the mean value results in the degradation of coherence in SG [45]. However, fortunately, the effects of these noises on coherence degradation also depend on the duration of the input pulse and propagation length, thus a short fiber pumped with a short pulse can be used to improve coherence characteristics. In our work, the high nonlinearity of the nitrobenzene-core PCF allows obtaining SG with a broad spectral width at a very short propagation length of 5 cm when pumped by ultra-short laser pulses (120 fs or 90 fs). Therefore, the effects of the noises can be neglected. Importantly, for these fiber length and pump pulse duration parameters, Raman scattering can be practically excluded, due to its delay compared to Kerr nonlinearity. Some other noise sources, on the other hand, i.e. phase diffusion [46], do not play any role when a mode-locked laser source is used (or assumed in a simulation). We note that physical conditions not included in our numerical simulations, such as the limited dynamic range of measurement setup, higher order mode or polarization mode component excitation, and their detrimental interactions over this short length of fiber, could contribute to a lowering of coherence from close to 1.0 shown in figures 6–8, down to around 0.8, which has been reported e.g. for normal-dispersion coherent SG in all-solid glass PCF experimentally [47].

An optimized fiber structure should be compatible with a preferred femtosecond laser source, which means low absolute dispersion for the central pump wavelength and low attenuation. The fibers $\#F_1$, $\#F_2$, and $\#F_3$ are optimized for sources operating at 1030 nm and 1560 nm, respectively. However, it is possible to choose a fiber with different Λ and f that is compatible with sources operating at different wavelengths. For example, it should be possible to achieve all-normal SG in the fiber with $\Lambda = 1.5$ μm and $f = 0.3$, shown in figure 3(b), pumped with Tm- or Ho-doped lasers at ~2 μm.

5. Conclusions

Of the many highly nonlinear liquids that were proposed so far, nitrobenzene seems to be a particularly good candidate for SG in liquid-core PCFs. Its nonlinearity is higher than that of fused silica ($n_2 = 2.74 \times 10^{-20}$ m^2 W^{-1}), comparable with such liquids as $CHCl_3$ ($n_2 = 1.64 \times 10^{-19}$ m$^2 \cdot$W^{-1}) and CCl_4 (1.53×10^{-19} m^2 W^{-1}), but lower than that of toluene ($n_2 = 1.6 \times 10^{-18}$ m^2 W^{-1}) and CS_2 ($n_2 = (4.3–5.1) \times 10^{-18}$ m^2 W^{-1}).

We have optimized the geometrical parameters of the PCFs with a nitrobenzene-filled core to obtain both all-normal and anomalous dispersion characteristics. The PCF parameters allow for high coupling efficiency with standard femtosecond fibers and for high fiber nonlinearity. Due to the latter property, highly coherent SG is obtained for short segments of fibers, on the level of single-digit centimeters, with pulse energy as low as 0.1 nJ and pulse duration 90 fs or 120 fs. Two of our fibers, $\#F_1$ and $\#F_2$, should allow for SC in the range of 0.8–1.8 μm or 0.8–2.1 μm, respectively, while the third $\#F_3$ allows for SC in the range of 1.3–2.3 μm. Standard femtosecond fiber lasers can be used for SG in all proposed PCFs. An optimized

fiber structure should be compatible with a preferred femtosecond laser source, which means low absolute dispersion for the central pump wavelength and low attenuation. The fiber $\#F_1$ is optimized for sources operating at 1030 nm, while the fibers $\#F_2$ and $\#F_3$ are optimized for sources operating at 1560 nm. However, it is possible to choose a fiber with different Λ and f, that is compatible with sources operating at different wavelengths. For example, it should be possible to achieve all-normal SG in the fiber with $\Lambda = 1.5$ μm, and $f = 0.3$, shown in figure 3(b), pumped with Tm- or Ho-doped lasers at ~2 μm.

All proposed fibers are good candidates for all-fiber SC sources as an alternative to glass-core fibers, since the nonlinearity of nitrobenzene is higher than that of silica. Note that the all-fiber systems are robust, shock-proof, and do not comprise axis adjustment mechanics nor additional pulse compressors.

Acknowledgments

The authors acknowledge Narodowe Centrum Nauki (NCN) (UMO-2016/21/M/ST2/00261); the Foundation for Polish Science, (FNP) (POIR. 04.04.00-1C74/16) Team Programme co-financed by the European Regional Development Fund under the Smart Growth Operational Programme (SG OP), Priority Axis IV; H2020 ACTPHAST 4.0 (Grant No. 779472); Vietnam's Ministry of Education and Training (B2017-TDV-03); Uniwersytet Warszawski (UW) (statutory research).

References

[1] Knight J C, Birks T A, Russell P S J and Atkin D M 1996 All-silica single-mode optical fiber with photonic crystal cladding *Opt. Lett.* **21** 1547–9
[2] Birks T A, Knight J C and Russell P S J 1997 Endlessly single-mode photonic crystal fiber *Opt. Lett.* **22** 961–3
[3] Cregan R F, Mangan B J, Knight J C, Birks T A, Russell P S J, Roberts P J and Allan D C 1999 Single-mode photonic band gap guidance of light in air *Science* **285** 1537–9
[4] Ortigosa-Blanch A, Knight J C, Wadsworth W J, Arriaga J, Mangan B J, Birks T A and Russell P S J 2000 Highly birefringent photonic crystal fibers *Opt. Lett.* **25** 1325–7
[5] Knight J C, Arriaga J, Birks T A, Ortigosa-Blanch A, Wadsworth W J and Russell P S J 2000 Anomalous dispersion in photonic crystal fiber *IEEE Photonics Technol. Lett.* **12** 807–9
[6] Dabas B and Sinha R K 2010 Dispersion characteristic of hexagonal and square lattice chalcogenide As_2Se_3 glass photonic crystal fiber *Opt. Commun.* **283** 1331–7
[7] Baggett J C, Monro T M, Furusawa K and Richardson D J 2001 Comparative study of large-mode holey and conventional fibers *Opt. Lett.* **26** 1045–7
[8] Luan F, George A K, Hedley T D, Pearce G J, Bird D M, Knight J C and Russell P S J 2004 All-solid photonic bandgap fiber *Opt. Lett.* **29** 2369–71
[9] Tuchin V V, Skibina Yu S, Beloglazov V I, Chainikov M V, Skibina N B, Mikhailova N A, Zhestkov P M and Silokhin I Yu 2008 Sensor properties of hollow-core photonic crystal fibers *Tech. Phys. Lett.* **34** 663
[10] Chen Z-H, Yang F, Chen D-J and Cai H-W 2017 A frequency-stabilized laser based on a hollow-core photonic crystal fiber CO_2 gas cell and its application scheme *Laser Phys.* **27** 045102
[11] Buczynski R, Pysz D, Stepien R, Waddie A J, Kujawa I, Kasztelanic R, Franczyk M and Taghizadeh M R 2011 Supercontinuum generation in photonic crystal fibers with nanoporous core made of soft glass *Laser Phys. Lett.* **8** 443–8
[12] Ebnali-Heidari M, Dehghan F, Saghaei H, Koohi-Kamali F and Moravvej-Farshi M K 2012 Dispersion engineering of photonic crystal fibers by means of fluidic infiltration *J. Mod. Opt.* **59** 1384–90
[13] Pniewski J, Stefaniuk T, Van H L, Long V C, Van L C, Kasztelanic R, Stepniewski G, Ramaniuk A, Trippenbach M and Buczyński R 2016 Dispersion engineering in nonlinear soft glass photonic crystal fibers infiltrated with liquids *Appl. Opt.* **55** 5033–40
[14] Du F, Lu Y-Q and Wu S-T 2004 Electrically tunable liquid-crystal photonic crystal fiber *Appl. Phys. Lett.* **85** 2181–3
[15] Van H L, Buczynski R, Long V C, Trippenbach M, Borzycki K, Manh A N and Kasztelanic R 2018 Measurement of temperature and concentration influence on the dispersion of fused silica glass photonic crystal fiber infiltrated with water–ethanol mixture *Opt. Commun.* **407** 417–22
[16] Vieweg M, Gissibl T, Pricking S, Kuhlmey B T, Wu D C, Eggleton B J and Giessen H 2010 Ultrafast nonlinear optofluidics in selectively liquid-filled photonic crystal fibers *Opt. Express* **18** 25232–40
[17] Maji P S and Roy Chaudhuri P 2014 Supercontinuum generation in ultra-flat near zero dispersion PCF with selective liquid infiltration *Optik* **125** 5986–92
[18] Churin D, Nguyen T N, Kieu K, Norwood R A and Peyghambarian N 2013 Mid-IR supercontinuum generation in an integrated liquid-core optical fiber filled with CS_2 *Opt. Mater. Express* **3** 1358–64
[19] Kedenburg S, Gissibl T, Steinle T, Steinmann A and Giessen H 2015 Towards integration of a liquid-filled fiber capillary for supercontinuum generation in the 1.2–2.4 μm range *Opt. Express* **23** 8281–9
[20] Lanh V C, Anuszkiewicz A, Ramaniuk A, Kasztelanic R, Xuan K D, Long V C, Trippenbach M and Buczyński R 2017 Supercontinuum generation in photonic crystal fibres with core filled with toluene *J. Opt.* **19** 125604
[21] Van Le H, Cao V L, Nguyen H T, Nguyen A M, Buczyński R and Kasztelanic R 2018 Application of ethanol infiltration for ultra-flattened normal dispersion in fused silica photonic crystal fibers *Laser Phys.* **28** 115106
[22] Dinh Q H, Pniewski J, Van H L, Ramaniuk A, Long V C, Borzycki K, Xuan K D, Klimczak M and Buczynski R 2018 Optimization of optical properties of photonic crystal fibers infiltrated with carbon tetrachloride for supercontinuum generation with subnanojoule femtosecond pulses *Appl. Opt.* **57** 3738–46
[23] Raei R 2018 Supercontinuum generation in organic liquid–liquid core-cladding photonic crystal fiber in visible and near-infrared regions *J. Opt. Soc. Am.* B **35** 323–30
[24] Chemnitz M, Gebhardt M, Gaida C, Stutzki F, Kobelke J, Limpert J, Tünnermann A and Schmidt M A 2017 Hybrid soliton dynamics in liquid-core fibres *Nat. Commun.* **8** 42
[25] Chemnitz M, Gaida C, Gebhardt M, Stutzki F, Kobelke J, Nnermann A T, Limpert J and Schmidt M A 2018 Carbon chloride-core fibers for soliton mediated supercontinuum generation *Opt. Express* **26** 3221–35
[26] Lanh C V, Hoang V T, Long V C, Borzycki K, Xuan K D, Quoc V T, Trippenbach M, Buczyński R and Pniewski J 2019 Optimization of optical properties of photonic crystal fibers infiltrated with chloroform for supercontinuum generation *Laser Phys.* **29** 075107
[27] Wang C-C, Li W-M, Li N and Wang W-Q 2017 Numerical simulation of coherent visible-to-near-infrared

supercontinuum generation in the $CHCl_3$-filled photonic crystal fiber with 1.06 μm pump pulses *Opt. Laser Technol.* **88** 215–21
[28] Zhang H, Chang S, Yuan J and Huang D 2010 Supercontinuum generation in chloroform-filled photonic crystal fibers *Optik* **121** 783–7
[29] Zhao P, Reichert M, Benis S, Hagan D J and van Stryland E W 2018 Temporal and polarization dependence of the nonlinear optical response of solvents *Optica* **5** 583–94
[30] Hoang V T *et al* 2018 All-normal dispersion supercontinuum generation in photonic crystal fibers with large hollow cores infiltrated with toluene *Opt. Mater. Express* **8** 3568–82
[31] Hoang V T *et al* 2019 Supercontinuum generation in an all-normal dispersion large core photonic crystal fiber infiltrated with carbon tetrachloride *Opt. Mater. Express* **9** 2264–78
[32] Zhang R, Teipel J and Giessen H 2006 Theoretical design of a liquid-core photonic crystal fiber for supercontinuum generation *Opt. Express* **14** 6800–12
[33] Lumerical Solutions, Inc. (http://lumerical.com)
[34] Saitoh K, Koshiba M, Hasegawa T and Sasaoka E 2003 Chromatic dispersion control in photonic crystal fibers: application to ultra-flattened dispersion *Opt. Express* **11** 843–52
[35] Dudley J M, Genty G and Coen S 2006 Supercontinuum generation in photonic crystal fiber *Rev. Mod. Phys.* **78** 1135–84
[36] Zhao P, Reichert M, Ensley T R, Shensky W M III, Mott A G, Hagan D J and Van Stryland E W 2016 Nonlinear refraction dynamics of solvents and gases *Nonlinear Frequency Generation and Conversion: Materials, Devices, and Applications XV* vol 9731 p 97310F
[37] Dudley J M and Coen S 2002 Coherence properties of supercontinuum spectra generated in photonic crystal and tapered optical fibers *Opt. Lett.* **27** 1180–2
[38] Gaeta A L 2002 Nonlinear propagation and continuum generation in microstructured optical fibers *Opt. Lett.* **27** 924–6
[39] Agrawal G 2012 *Nonlinear Fiber Optics* (New York: Academic)
[40] Heidt A M, Feehan J S, Price J H V and Feurer T 2017 Limits of coherent supercontinuum generation in normal dispersion fibers *J. Opt. Soc. Am.* B **34** 764–75
[41] Tran T X and Biancalana F 2009 Dynamics and control of the early stage of supercontinuum generation in submicron-core optical fibers *Phys. Rev.* A **79** 065802
[42] Wang F, Yao C F, Li C Z, Jia Z X, Li Q, Wu C F, Ohishi Y, Qin W P and Qin G S 2018 Experimental observation of breathing solitons and a third harmonic in a tapered photonic crystal fiber *Laser Phys.* **28** 025102
[43] Gonzalo I B and Bang O 2018 Role of the Raman gain in the noise dynamics of all-normal dispersion silica fiber supercontinuum generation *J. Opt. Soc. Am.* B **35** 2102–10
[44] Gonzalo I B, Engelsholm R D, Sørensen M P and Bang O 2018 Polarization noise places severe constraints on coherence of all-normal dispersion femtosecond supercontinuum generation *Sci. Rep.* **8** 6579
[45] Genier E, Bowen P, Sylvestre T, Dudley J M, Moselund P and Bang O 2019 Amplitude noise and coherence degradation of femtosecond supercontinuum generation in all-normal-dispersion fibers *J. Opt. Soc. Am.* B **36** A161
[46] Frosz M H 2010 Validation of input-noise model for simulations of supercontinuum generation and rogue waves *Opt. Express* **18** 14778–87
[47] Klimczak M, Soboń G, Kasztelanic R, Abramski K M and Buczyński R 2016 Direct comparison of shot-to-shot noise performance of all normal dispersion and anomalous dispersion supercontinuum pumped with sub-picosecond pulse fiber-based laser *Sci. Rep.* **5** 19284